Journal of ELECTRONIC MATERIALS, Vol. 43, No. 1, 2014
DOI: 10.1007/s11664-013-2829-z

Optical Properties of Al_xO_y/Ni/Al_xO_y Multilayered Absorber Coatings Prepared by Reactive DC Magnetron Sputtering

T.K. TSAI,[1,3] S.J. HSUEH,[2] and J.S. FANG[1]

1.—Department of Materials Science and Engineering, National Formosa University, Huwei, Yunlin 632, Taiwan. 2.—Department of Materials Science and Engineering, National Chiao Tung University, Hsinchu 300, Taiwan. 3.—e-mail: dktsai@sunws.nfu.edu.tw

Al_xO_y/Ni/Al_xO_y multilayered absorber coatings were deposited on stainless-steel substrates using reactive direct-current (DC) magnetron sputtering. Al_xO_y films with different morphologies, structures, and optical transmittances were obtained by varying the DC power and oxygen flux. The Al_xO_y films were characterized using field-emission scanning electron microscopy, transmission electron microscopy, energy-dispersive x-ray spectrometry, grazing-incidence x-ray diffraction, and ultraviolet/visible/near-infrared spectrophotometry. The effect of the thickness of the Al_xO_y films on the optical properties of Al_xO_y/Ni/Al_xO_y coatings was also investigated. Experimental results show that the thermal emittance of the Al_xO_y/Ni/Al_xO_y multilayered absorber coatings decreases as the thickness of the Al_xO_y top layer is decreased. The Al_xO_y/Ni/Al_xO_y multilayered absorber coating with 70-nm-thick Al_xO_y top and bottom layers showed the best optical properties. The thermal stability of the Al_xO_y/Ni/Al_xO_y multilayered absorber coating in which the Al_xO_y films were deposited at conditions of 150 W and 8 sccm O_2 was at least 12 h when the multilayered absorber was annealed at 400°C in air.

Key words: Al_xO_y/Ni/Al_xO_y, multilayered absorber coating, sputtering, absorptance, thermal emittance

INTRODUCTION

A solar absorber is an efficient solar photothermal energy converter because the absorber has high absorptance (α) in the solar irradiation region (0.3 μm to 2.5 μm) and low thermal emission (ε) in the infrared region (2.5 μm to 20 μm). Therefore, it can be widely used in solar collection devices. As a solar collection device, a solar absorber must have high thermal and chemical stability in adverse circumstances. Generally, a solar absorber consists of a spectrally selective absorber coating, which absorbs the solar radiation but transmits infrared (IR) radiation, and a highly IR-reflective metal substrate. Intrinsic,[1] semiconductor,[2] multilayer,[3,4] and metal–dielectric composite coatings[5,6] have been proposed as spectrally selective absorber coatings for solar absorbers. Of these absorber coatings, multilayered absorber coatings are most attractive, because of their excellent optical properties and high thermal stability.[7,8]

Multilayered absorber coatings are a combination of complex dielectric–metal multilayers, in which the solar radiation is trapped between the alternate dielectric and metal layers. Several dielectric/translucent metal/dielectric multilayered absorber coatings deposited on IR-reflective metal substrates have been reported in the literature for high-temperature applications.[9–13] The topmost dielectric film acts as an antireflection layer to decrease the reflection of incident light, and also as a passivation layer in adverse environments. The incident solar radiation is absorbed by multiple reflections between the translucent metal film and the metal substrate. Thornton et al.[9] studied the thermal stability of Al_2O_3/M/Al_2O_3 multilayered absorber coatings with M layers of Cr, Ni, Mo, Ta, and a Pt-Al_2O_3 cermet, and with Al_2O_3 layers deposited using both direct radiofrequency (RF) sputtering of

(Received April 26, 2013; accepted September 26, 2013; published online October 29, 2013)

alumina and reactive sputtering of aluminum. Barshilia et al.[10,11] investigated the optical properties and thermal stability of pulsed-sputter-deposited $Al_xO_y/Al/Al_xO_y$ and $Cr_xO_y/Cr/Cr_2O_3$ multilayered absorber coatings. The compositions and thicknesses of the individual component layers were optimized to achieve high α and low ε values. Selvakumar et al.[12] reported that pulsed-sputter-deposited $HfO_x/Mo/HfO_2$ coatings on a copper substrate and a stainless-steel substrate had high α and low ε values. The $HfO_x/Mo/HfO_2$ coatings deposited on the copper substrate were thermally stable in air, up to 400°C for 2 h. The $Mo/HfO_x/Mo/HfO_2$ coatings deposited on the stainless-steel substrate were thermally stable up to 500°C in air and up to 800°C in vacuum. Nuru et al.[13] studied $Al_xO_y/Pt/Al_xO_y$ multilayered absorber coatings, using optical simulations to optimize their optical properties. These multilayered absorber coatings were produced using a physical vapor deposition (PVD) method, such as e-beam evaporation and sputtering deposition. Sputtering deposition is widely used for deposition of spectrally selective absorber coatings over large areas.[8,14,15]

Al_2O_3 has high thermal and chemical stability, and excellent dielectric properties, making it one of the most attractive dielectric materials for absorber coatings.[16,17] Al_2O_3 film has a wide bandgap and a low refractive index, making it fully transparent over the wavelength region of interest for a solar absorber.[18] However, the optical properties of Al_2O_3 films are dependent on the deposition conditions, which determine the constituted phase, chemical composition, and morphology of the Al_2O_3 films.[19–21] The thickness of the Al_2O_3 film also determines the shape and position of the spectral reflectance curve.[13]

This work determined the optical properties and thermal stability of $Al_xO_y/Ni/Al_xO_y$ multilayered absorber coatings deposited on a stainless-steel substrate using reactive DC magnetron sputtering. The effect of the DC power and oxygen flux on the morphology, structure, and optical transmittance of the Al_xO_y films was determined, and the effect of the thickness of the Al_xO_y films on the optical properties of the $Al_xO_y/Ni/Al_xO_y$ multilayered absorber coatings was also evaluated.

EXPERIMENTAL PROCEDURES

Al_xO_y films were prepared on well-cleaned glass substrates and silicon wafer substrates at room temperature using a reactive DC magnetron sputtering system. A 2-inch-diameter Al target with purity of 99.999% was used as a sputtering target. Prior to deposition, the process chamber was evacuated using a turbomolecular pump to pressure of 3×10^{-6} torr. The Al target was sputter-cleaned for 10 min before Al_xO_y film deposition to remove the surface contaminants of the target. Al_xO_y films were deposited in a mixture of Ar and O_2 plasma, adjusting the DC power (150 W to 250 W) and O_2 flow rate (2 sccm to 8 sccm). The Ar flow rate was kept at 20 sccm controlled by a mass flow meter, and the working pressure was maintained at 3×10^{-3} torr controlled by a gas outlet valve during the deposition process. $Al_xO_y/Ni/Al_xO_y$ multilayered absorber coatings with various thicknesses of top and bottom Al_xO_y layers were deposited on a cleaned 304 stainless-steel substrate, adjusting the deposition time. The thickness of the Ni middle layer in the $Al_xO_y/Ni/Al_xO_y$ multilayered absorber coatings was 20 nm.

A field-emission scanning electron microscope (FESEM, JSM-7500F; JEOL Ltd.) was used to study the surface morphology of the Al_xO_y films. Cross-sectional micrographs of Al_xO_y films and $Al_xO_y/Ni/Al_xO_y$ multilayered absorber coatings were obtained by using a transmission electron microscope (TEM, JEM-2010; JEOL Ltd.). Elemental analysis of the Al_xO_y films was carried out using the TEM equipped with an Oxford Link energy-dispersive x-ray spectrometry. Phase identification of various Al_xO_y films was carried out by grazing-incidence x-ray diffraction (GIXRD) analysis (D8 Advance; Bruker Ltd.). The optical transmittance of the Al_xO_y films deposited on glass substrates was measured in the wavelength range from 300 nm to 2500 nm by ultraviolet/visible/near-infrared (UV/VIS/NIR) spectrophotometry (V-570; JASCO). The refractive index of the studied Al_xO_y films was measured using an ellipsometer (M-2000; J. A. Woollam Co., Inc.) in the wavelength range from 350 nm to 1200 nm. The normal reflectance of the $Al_xO_y/Ni/Al_xO_y$ coatings deposited on stainless-steel substrates was measured in the wavelength range from 300 nm to 20,000 nm. The UV/VIS/NIR spectrophotometer embedded with a $BaSO_4$-coated integrating sphere was applied for the 300 nm to 2500 nm wavelength region. A Fourier-transform infrared (FTIR) spectrophotometer (Nexus 470; Thermo Nicolet) with an integrating sphere was used for the spectral range between 2500 nm and 20,000 nm. The normal solar absorptance and normal thermal emittance were calculated from the reflectance measurements according to the Duffie and Beckman methodology[22] using the following equations:

$$\alpha = \int_{300\text{nm}}^{2500\text{nm}} \frac{I_{\text{sol}}(\lambda)(1 - R(\lambda))\mathrm{d}\lambda}{I_{\text{sol}}(\lambda)\mathrm{d}\lambda}, \quad (1)$$

$$\varepsilon = \int_{2500\text{nm}}^{20{,}000\text{nm}} \frac{I_{\text{p}}(\lambda)(1 - R(\lambda))\mathrm{d}\lambda}{I_{\text{p}}(\lambda)\mathrm{d}\lambda}, \quad (2)$$

where I_{sol} is the AM1.5 normal solar irradiance and I_{p} is the Planck black-body distribution at 100°C. Tests were performed at 400°C in air to evaluate the thermal stability of the studied $Al_xO_y/Ni/Al_xO_y$ multilayered absorber coatings.

RESULTS AND DISCUSSION

Characterization of Al_xO_y Films

The sputtering power and oxygen flow rate affect the composition, structure, and optical properties of Al_xO_y films deposited using reactive DC magnetron sputtering. The Al_xO_y films deposited using various DC powers and oxygen flow rates are denoted as A(DC power/oxygen flow rate); For instance, an Al_xO_y film deposited using 150 W and 2 sccm O_2 is denoted as A(150/2) film.

Figure 1 shows SEM micrographs of as-deposited A(150/2), A(250/2), A(150/8), and A(250/8) films. Figure 1a and b show that the A(150/2) and A(250/2) films have a flake-like morphology. Many voids (marked with circles) are distributed across the surfaces of the A(150/2) and A(250/2) films. The roughness of the Al_xO_y flake increases as the DC power is increased from 150 W to 250 W. In contrast to the A(150/2) and A(250/2) films, the surface morphologies of the A(150/8) and A(250/8) films, which were deposited using an O_2 flow rate of 8 sccm, are more even and dense (Fig. 1c, d). Figure 2a and b show TEM cross-sectional images of the as-deposited A(150/2) and A(250/2) films, respectively. Many voids are seen in the as-deposited A(150/2) and A(250/2) films, indicating that the structure of the A(150/2) and A(250/2) films is loose. The TEM and SEM results show that the Al_xO_y films deposited using an oxygen flow rate of 2 sccm have a rough surface and a loose structure. The A(250/2) film has a rougher and looser structure than the A(150/2) film. Figure 2c shows a TEM cross-sectional image of the as-deposited A(150/8) film. The A(150/8) film has a dense structure, and no voids are seen. Increasing the sputtering power and decreasing the oxygen partial pressure result in an increase in the deposition rate of Al_xO_y film. The differences in the surface morphology and structure of the Al_xO_y films deposited using different sputtering powers and oxygen flow rates may be due to the difference in the deposition rates. The diffraction pattern of the A(150/2) film is a broadened ring, as shown in Fig. 2d, which indicates that the A(150/2) film has an amorphous structure. Other Al_xO_y films in this study exhibit diffraction patterns that are similar to that of the A(150/2) film. The phase of the Al_xO_y films was further confirmed by GIXRD analysis, as shown in Fig. 3. No diffraction peak for Al_2O_3 is observed, which shows that all of the studied Al_xO_y films are amorphous. The results of the GIXRD analysis correlate well with the TEM observations. Related studies have also observed that sputtered Al_xO_y films exhibit an amorphous structure.[23,24] The resultant amorphous Al_xO_y film is attributed to a low substrate temperature during sputtering, because the crystallization temperature of aluminum oxide exceeds 900°C. The aluminum content in the A(150/2) film is about 43 at.% to 47 at.%, whereas that in the A(150/8) film is about

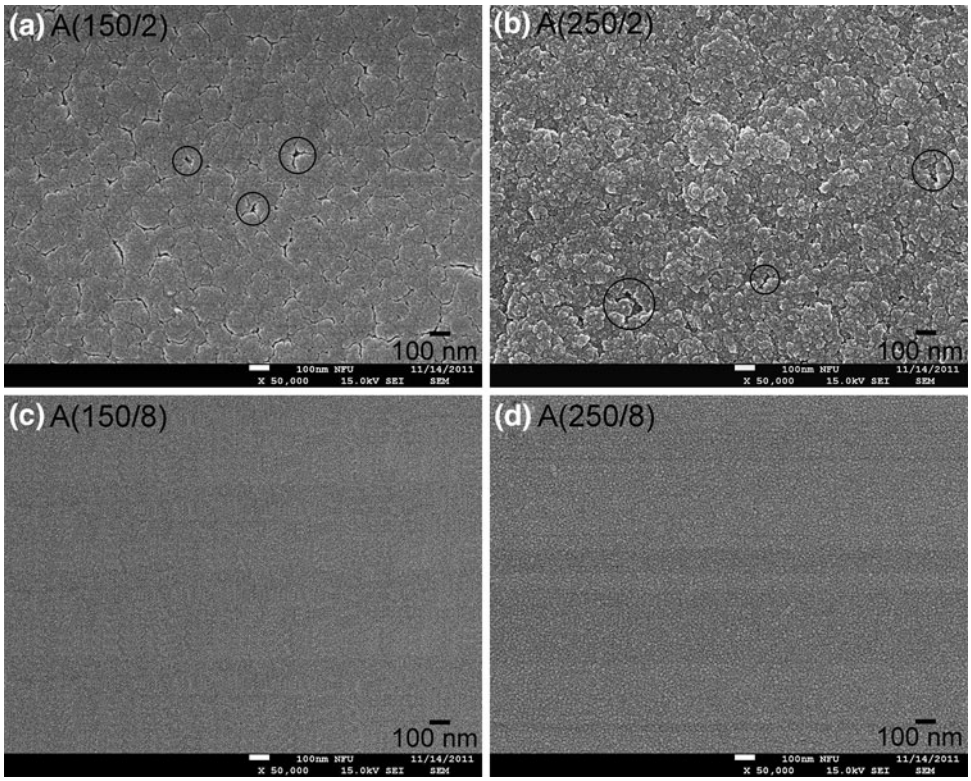

Fig. 1. SEM surface morphologies of as-deposited A(150/2) (a), A(250/2) (b), A(150/8) (c), and A(250/8) (d) films.

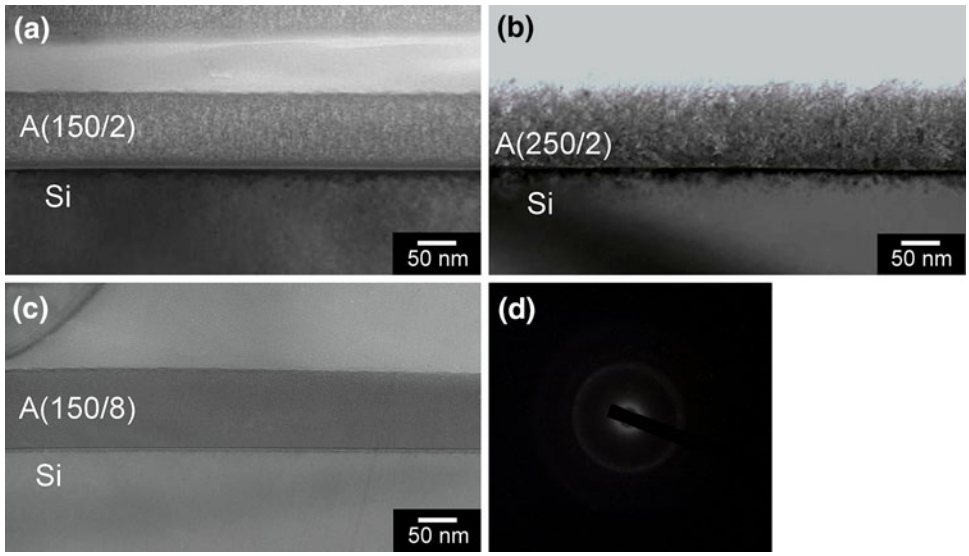

Fig. 2. TEM cross-sectional micrographs of as-deposited A(150/2) (a), A(250/2) (b), and A(150/8) (c) films, and diffraction pattern of as-deposited A(150/2) (d).

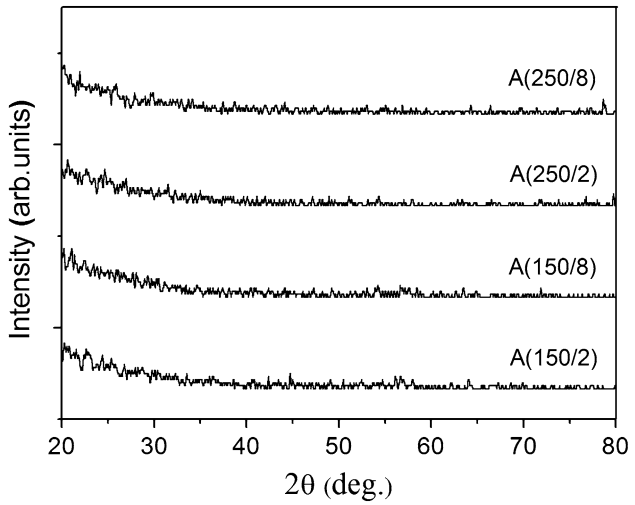

Fig. 3. GIXRD patterns of the studied Al_xO_y films.

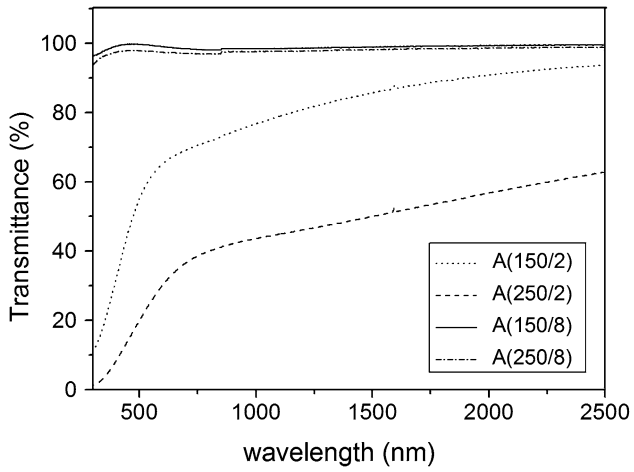

Fig. 4. Spectral transmittance curves of the studied Al_xO_y films.

30 at.% to 32 at.%. The aluminum content in the Al_xO_y film increases slightly, by about 3 at.% to 5 at.%, when the DC power is increased from 150 W to 250 W, for the same oxygen flux. The composition analysis also shows that the as-deposited Al_xO_y films have a nonstoichiometric composition.

Figure 4 shows the optical transmittance, for wavelengths from 300 nm to 2500 nm, of the Al_xO_y films deposited on glass substrates. The A(150/2) and A(250/2) films have low transmittance values, and the transmittance decreases with an increase in the sputtering power from 150 W to 250 W. The optical transmittances of the A(150/8) and A(250/8) films are nearly 100%, which shows that the A(150/8) and A(250/8) films exhibit typical dielectric behavior. The difference in the optical transmittance for the Al_xO_y films deposited using an O_2 flow rate of 2 sccm versus 8 sccm may be due to the distinct structures of the films. As mentioned above, the A(150/2) and A(250/2) films have a loose structure and a rough surface. A loose structure embedded with voids interferes with the incident light, so there is an increase in light absorption. A rough surface also reflects incident light in all directions and causes an increase in the absorption capacity for incident light due to cavity trapping. Therefore, the A(150/2) and A(250/2) films have low optical transmittance.

Optical Properties of Al_xO_y/Ni/Al_xO_y Multilayered Absorber Coatings

As well as the composition and structure of Al_xO_y films, the thickness of the Al_xO_y films also affects the optical properties of the Al_xO_y/Ni/Al_xO_y coatings.

Table I. Labels of $SS/Al_xO_y/Ni/Al_xO_y$ multilayer absorbers with various Al_xO_y top and bottom layers

Sample Label	$SS/Al_xO_y/Ni/Al_xO_y$ Multilayer Absorber
A1	SS/A(250/2)-120 nm/Ni-20 nm/A(250/2)-120 nm
A2	SS/A(250/2)-120 nm/Ni-20 nm/A(250/2)-70 nm
A3	SS/A(250/2)-70 nm/Ni-20 nm/A(250/2)-120 nm
A4	SS/A(250/2)-70 nm/Ni-20 nm/A(250/2)-70 nm
B1	SS/A(150/8)-70 nm/Ni-20 nm/A(150/8)-90 nm
B2	SS/A(150/8)-70 nm/Ni-20 nm/A(150/8)-70 nm
B3	SS/A(150/8)-70 nm/Ni-20 nm/A(150/8)-40 nm

SS stainless steel.

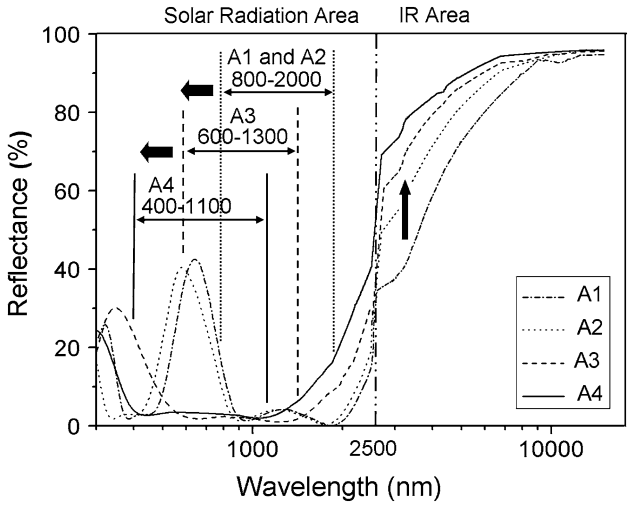

Fig. 5. Spectral reflectance curves of the A1, A2, A3, and A4 samples.

In this study, A(250/2) and A(150/8) films of different thicknesses were used in the stacked $Al_xO_y/Ni/Al_xO_y$ multilayered absorber coatings, in order to evaluate the optical properties. Table I lists the sample labels of the studied $Al_xO_y/Ni/Al_xO_y$ multilayered absorber coatings. To prevent reflection of incident light, the optical thickness (refractive index × film thickness) of a single-layer film must be an odd number of quarter incident wavelengths. The main absorption wavelength range for solar irradiation is around 400 nm to 800 nm. Within this wavelength range, the refractive index of the studied Al_xO_y films is 1.76 to 1.62, as determined by ellipsometric measurements. Therefore, 70-nm- and 120-nm-thick A(250/2) films were used for the $Al_xO_y/Ni/Al_xO_y$ multilayered absorber coatings. Figure 5 shows the spectral reflectance curves for the A(250/2) film with A1, A2, A3, and A4 thickness stacking. The main absorption ranges of the A1 and A2 samples, stacked with 120-nm Al_xO_y bottom layers, were located within the range of 800 nm to 2000 nm, while those of the A3 and A4 samples,

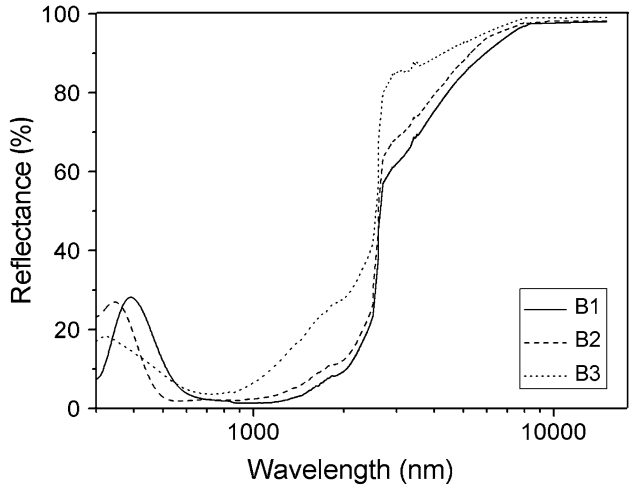

Fig. 6. Spectral reflectance curves of the B1, B2, and B3 samples.

stacked with 70-nm Al_xO_y bottom layers, were located within the range of 600 nm to 1300 nm and 400 nm to 1100 nm, respectively. The absorption range shifts to shorter wavelength as the thickness of the bottom Al_xO_y layer is reduced from 120 nm to 70 nm. This result was also noted in the study by Kumar et al.[25] They grew Al_2O_3 films with thicknesses of 400 nm, 300 nm, and 200 nm on a soda-lime glass substrate, in order to investigate the optical properties of these Al_2O_3 films. The A1 and A2 samples have lower reflectance in the IR wavelength region than that of the A3 and A4 samples, as shown in Fig. 5. Table II lists the α and ε values for A1, A2, A3, and A4 samples. The α/ε values for the A1 and A2 samples are 0.844/0.121 and 0.852/0.087, respectively. The α/ε values for both the A3 and A4 samples are improved, to 0.928/0.079 and 0.936/0.060, respectively. The optical measurements indicate that a multilayered coating with a 70-nm Al_xO_y bottom layer has higher solar absorptance and lower thermal emittance than a multilayered coating with a 120-nm bottom layer. The optical thickness of the 120-nm-thick Al_xO_y bottom layer is about 190 nm to 210 nm, and the absorption ranges of the A1 and A2 samples are beyond 800 nm. The optical thickness reduces to 115 nm to 125 nm when the thickness of the Al_xO_y film is decreased to 70 nm. The absorption ranges of the A3 and A4 samples shift to 600 nm to 1300 nm and 400 nm to 1100 nm, covering the main wavelength range of solar radiation. Therefore, the absorptance values of the A3 and A4 samples are higher than those of the A1 and A2 samples.

A 70-nm-thick A(150/8) bottom layer and 40-nm-, 70-nm-, and 90-nm-thick A(150/8) top layers were used to stack further $Al_xO_y/Ni/Al_xO_y$ multilayered absorber coatings, denoted as B series samples in Table I, to determine the effect of the thickness of the top Al_xO_y layer on the optical properties of the $Al_xO_y/Ni/Al_xO_y$ coatings. Figure 6 shows the spectral reflectance curves for the B1, B2, and B3

Table II. Optical properties (α/ε) of A and B series samples

	A1	A2	A3	A4
α/ε	0.844/0.121	0.852/0.087	0.928/0.079	0.936/0.060
	B1	**B2**		**B3**
α/ε	0.914/0.055	0.932/0.038		0.893/0.026

Table III. Optical properties of A4 and B2 samples before and after thermal stability test

	As-Deposited α/ε	12 h α/ε	60 h α/ε	120 h α/ε
A4	0.936/0.060	0.821/0.051	0.819/0.052	
B2	0.932/0.038	0.927/0.040	0.904/0.043	0.902/0.045

samples. The reflectance curve shifts to a short-wavelength region when the thickness of the Al_xO_y top layer is decreased from 90 nm (B1 sample) to 40 nm (B3 sample). Table II presents the α/ε values of B1, B2, and B3 samples. The α value increases slightly from 0.914 to 0.932 when the Al_xO_y top layer thickness is decreased from 90 nm to 70 nm, then decreases to 0.893 when the Al_xO_y top layer thickness is decreased to 40 nm. The ε value decreases from 0.055 to 0.026 when the thickness of the Al_xO_y top layer is decreased from 90 nm to 40 nm. The experimental results show that the B2 sample has an optimal α/ε value of 0.932/0.038. A decrease in the thermal emittance of the Al_xO_y/Ni/Al_xO_y multilayered absorber coatings with a thin Al_xO_y top layer is also found for the A series samples. Additionally, the best optical properties for an Al_xO_y/Ni/Al_xO_y multilayered absorber coating are found for the multilayered coating with 70-nm-thick top and bottom layers.

Thermal Stability Test

The A4 and B2 samples were chosen to evaluate the thermal stability. Table III lists the α and ε values for the A4 and B2 samples, before and after the thermal stability test. The α value for the A4 sample decreased significantly, from 0.936 to 0.821, while the ε value decreased slightly, from 0.060 to 0.051, when the sample was annealed at 400°C for 12 h in air. This shows that the optical properties of the A4 sample obviously decayed after annealing for 12 h. The optical properties of the A4 sample did not vary significantly when the heating duration was increased to 60 h. However, the optical properties of the B2 sample remained almost the same as those of the as-deposited sample when the sample was annealed at 400°C for 12 h. When the annealing time was increased to 60 h, the α value decreased, from 0.927 to 0.904, and the ε value increased slightly, from 0.040 to 0.043. The α/ε value for the B2 sample remained at 0.902/0.045, even after annealing at 400°C for 120 h. The thermal stability of the B2 sample is superior to that of the A4 sample.

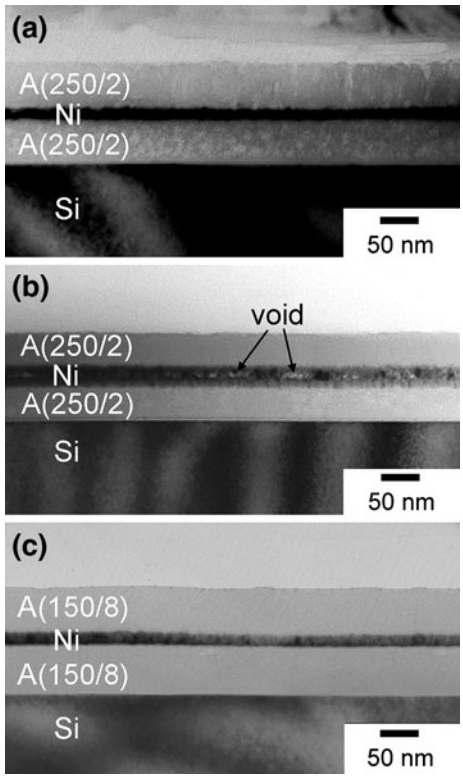

Fig. 7. TEM cross-sectional micrographs of A4 (b) and B2 (c) samples after 12 h of heating at 400°C in air, and A4 sample in the as-deposited state (a).

Figure 7a shows a TEM cross-sectional image of the as-deposited A4 sample. The top and bottom

A(250/2) films are loose, and so is the Ni film in the middle of the as-deposited A4 sample. Figure 7b shows that the A(250/2) films become dense and the Ni film becomes broad, with several voids, when the films are annealed at 400°C for 12 h. Annealing induces changes in the morphology and thickness of the A(250/2) and Ni films, so the structural variations in the heated A4 sample result in the decay of the optical properties. Figure 7c shows a TEM cross-sectional image of the B2 sample after 12 h of heat treatment. The heated B2 sample has a compact structure, so the optical properties of the B2 sample are maintained after the sample is annealed at 400°C for at least 12 h.

CONCLUSIONS

$Al_xO_y/Ni/Al_xO_y$ multilayered absorber coatings were deposited on stainless-steel substrates using reactive DC magnetron sputtering. All of the studied Al_xO_y films were amorphous and nonstoichiometric. The A(250/2) film has a loose structure and low optical transmittance. Conversely, the A(150/8) film has a dense structure and high optical transmittance of nearly 100%. A(250/2) and A(150/8) films of different thicknesses were used in stacked $Al_xO_y/Ni/Al_xO_y$ multilayered absorber coatings. The experimental results show that the thermal emittance of the $Al_xO_y/Ni/Al_xO_y$ multilayered absorber coatings decreases as the thickness of the Al_xO_y top layer is decreased. The $Al_xO_y/Ni/Al_xO_y$ multilayered absorber coating with 70-nm-thick Al_xO_y top and bottom layers showed the best optical properties. The thermal stability of the $Al_xO_y/Ni/Al_xO_y$ multilayered absorber coating is at least 12 h at 400°C in air, when the Al_xO_y films are deposited at conditions of 150 W and 8 sccm O_2.

ACKNOWLEDGEMENTS

The authors thank the National Science Council of the Republic of China, Taiwan, for financially supporting this research under Contract No. NSC 100-221-E-150-091.

REFERENCES

1. E. Randich and D.D. Allred, *Thin Solid Films* 83, 393 (1981).
2. B.O. Seraphin, *Thin Solid Films* 57, 293 (1979).
3. H.C. Barshilia, N. Selvakumar, K.S. Rajam, D.V. Sridhara Rao, and K. Muraleedharan, *Thin Solid Films* 516, 6071 (2008).
4. Y. Liu, C. Wan, and Y. Xue, *Sol. Energy Mater. Sol. Cells* 96, 131 (2012).
5. R.C. Juang, Y.C. Yeh, B.H. Chang, W.C. Chen, and T.W. Chung, *Thin Solid Films* 518, 5501 (2010).
6. H.C. Barshilia, P. Kumar, K.S. Rajam, and A. Biswas, *Sol. Energy Mater. Sol. Cells* 95, 1707 (2011).
7. C.E. Kennedy, *Review of Mid- to High-Temperature Solar Selective Absorber Materials, NREL/TP- 520-31267* (Golden, CO: National Renewable Energy Laboratory, 2002).
8. N. Selvakumar and H.C. Barshilia, *Sol. Energy Mater. Sol. Cells* 98, 1 (2012).
9. J.A. Thornton and J.L. Lamb, *Thin Solid Films* 96, 175 (1982).
10. H.C. Barshilia, N. Selvakumar, G. Vignesh, K.S. Rajam, and A. Biswas, *Sol. Energy Mater. Sol. Cells* 93, 315 (2009).
11. H.C. Barshilia, N. Selvakumar, and K.S. Rajam, *J. Appl. Phys.* 103, 023507 (2008).
12. N. Selvakumar, H.C. Barshilia, K.S. Rajam, and A. Biswas, *Sol. Energy Mater. Sol. Cells* 94, 1412 (2010).
13. Z.Y. Nuru, C.J. Arendse, S. Khamlich, and M. Maaza, *Vacuum* 86, 2129 (2012).
14. S. Zhao, E. Avendańo, K. Gelin, J. Lu, and E. Wäckelgård, *Sol. Energy Mater. Sol. Cells* 90, 308 (2006).
15. W. Graf, F. Brucker, L. Köhl, T. Tröscher, V. Wittwer, and L. Herlitze, *J. Non Cryst. Solids* 218, 380 (1997).
16. N. Selvakumar, N.T. Manikandanath, A. Biswas, and C. Barshilia, *Sol. Energy Mater. Sol. Cells* 102, 86 (2012).
17. A. Antonaia, A. Castaldo, M.L. Addonizio, and S. Esposito, *Sol. Energy Mater. Sol. Cells* 94, 1604 (2010).
18. G. Dingemans and W.M.M. Kessels, *J. Vac. Sci. Technol. A* 30, 040802 (2012).
19. J. Houska, J. Blazek, J. Rezek, and S. Proksova, *Thin Solid Films* 520, 5405 (2012).
20. O. Zywitzki and G. Hoetzsch, *Surf. Coat. Technol.* 94–95, 303 (1997).
21. Y. Chiba, Y. Abe, M. Kawamura, and K. Sasaki, *Vacuum* 84, 629 (2010).
22. J.A. Duffie and W.A. Beckman, *Solar Engineering of Thermal Processes*, 3rd edn. (New York, NY: Wiley, INC. 2006), p. 184.
23. S. Prasanna, G. Mohan Rao, S. Jayakumar, M.D. Kannan, and V. Ganesan, *Thin Solid Films* 520, 2689 (2012).
24. W.D. Sproul, D.J. Christie, and D.C. Carter, 2004 Society of Vacuum Coaters 505/856-7188 ISSN 0737-5921, *47th Annual Technical Conference Proceedings* (Dallas, TX, USA: April 24–29, 2004).
25. P. Kumar, M.K. Wiedmann, C.H. Winter, and I. Avrutsky, *Appl. Opt.* 48, 5407 (2009).